The thyroxine inactivating gene, type III deiodinase, suppresses multiple signaling centers in *Dictyostelium discoideum*

Shashi Prakash Singh [a], Ranjani Dhakshinamoorthy [a], Pundrik Jaiswal [a,1], Stefanie Schmidt [b], Sascha Thewes [b], Ramamurthy Baskar [a,*]

[a] *Department of Biotechnology, Bhupat and Jyoti Mehta School of Biosciences, Indian Institute of Technology-Madras, Chennai 600036, India*
[b] *Institute for Biology – Microbiology, Department of Biology, Chemistry, Pharmacy, Freie Universität Berlin, 14195 Berlin, Germany*

ABSTRACT

Thyroxine deiodinases, the enzymes that regulate thyroxine metabolism, are essential for vertebrate growth and development. In the genome of *Dictyostelium discoideum,* a single intronless gene (*dio3*) encoding type III thyroxine 5′ deiodinase is present. The amino acid sequence of *D. discoideum* Dio3 shares 37% identity with human T4 deiodinase and is a member of the thioredoxin reductase superfamily. *dio3* is expressed throughout growth and development and by generating a knockout of *dio3*, we have examined the role of thyroxine 5′ deiodinase in *D. discoideum. dio3⁻* had multiple defects that affected growth, timing of development, aggregate size, cell streaming, and cell-type differentiation. A prominent phenotype of *dio3⁻* was the breaking of late aggregates into small signaling centers, each forming a fruiting body of its own. cAMP levels, its relay, photo- and chemo-taxis were also defective in *dio3⁻*. Quantitative RT-PCR analyses suggested that expression levels of genes encoding adenylyl cyclase A (*acaA*), cAMP-receptor A (*carA*) and cAMP-phosphodiesterases were reduced. There was a significant reduction in the expression of CadA and CsaA, which are involved in cell–cell adhesion. The *dio3⁻* slugs had prestalk identity, with pronounced prestalk marker *ecmA* expression. Thus, Dio3 seems to have roles in mediating cAMP synthesis/relay, cell–cell adhesion and slug patterning. The phenotype of *dio3⁻* suggests that Dio3 may prevent the formation of multiple signaling centers during *D. discoideum* development. This is the first report of a gene involved in thyroxine metabolism that is also involved in growth and development in a lower eukaryote.

© 2014 Elsevier Inc. All rights reserved.

Introduction

During its life cycle *Dictyostelium discoideum* alternates between unicellular and multicellular modes of existence. In the growth phase, individual amoebae feed on bacteria and multiply (Bonner, 1967). If nutrients are limiting, multiplication ceases and hundreds to thousands of amoebae initiate a cAMP signal relay and form a multicellular aggregate (Konijn et al., 1969; Saran et al., 2002). The aggregate transforms to a motile slug and finally, a fruiting body that consists of a slender stalk capped by a cluster of spores. Cells at the anterior of the slug, the 'prestalk cells', differentiate to form the stalk of the fruiting body and the posterior 'prespore cells' form the spores (Raper, 1984; Williams, 2006). These cell types can be identified with a set of molecular markers (Gaudet et al., 2008).

In its immediate response to nutrient limitation *D. discoideum* amoebae secrete cAMP, which binds to a G-protein coupled cAMP receptor A (cARA) and activates adenylyl cyclase A (AcaA). Upon activation, AcaA catalyzes the conversion of ATP to cAMP, which is either secreted from the cell or used to initiate intracellular signaling events. cAMP levels are regulated, in part, by degradative phosphodiesterases, with RegA clearing excess intracellular cAMP, and extracellular phosphodiesterases PdsA and Pde4 doing likewise for secreted cAMP (Bader et al., 2006; Garcia et al., 2009; Shaulsky et al., 1998). The organized generation of cAMP pulses and their relay is important for both initiating aggregation and determining the size of the aggregate (Gomer et al., 2011; Gregor et al., 2010; Jaiswal et al., 2012).

Multicellular development also requires cell–cell adhesion and in *D. discoideum* this is mediated by cell surface glycoproteins such as CadA (Contact site B; gp24) and CsaA (Contact site A; gp80) (Roisin-Bouffay et al., 2000). CadA is a cadherin-dependent, EDTA-sensitive glycoprotein expressed in early development and CsaA is an EDTA-resistant glycoprotein that is expressed during aggregation (Kamboj et al., 1990). The expression of CadA and CsaA in turn depends on cAMP signaling.

---

* Corresponding author.
E-mail address: rbaskar@iitm.ac.in (R. Baskar).
[1] Present address: National Institutes of Diabetes and Digestive and Kidney Diseases (NIDDK), National Institutes of Health (NIH), Bethesda, MD 20892, USA.

Thyroxine deiodinases (Dio) are enzymes that catalyze the conversion of both active and inactive forms of thyroxine and have been reported in many vertebrates (Orozco et al., 2012). Thyroid gland secretes pro-hormone thyroxine (T4) into the blood stream, which transports T4 to target cells. The inactive T4 is converted to an active form, tri-iodothyronine (T3), by membrane-bound thyroxine deiodinases. These enzymes are expressed in a tissue specific manner in all vertebrates, from fish to mammals (Orozco et al., 2012).

In humans, three isoforms of Dio exist: Dio1, expressed in the liver and kidney; Dio2 in the heart, central nervous system and thyroid gland; and Dio3 in the fetus and placenta (Berry et al., 1991; Burrow et al., 1994; Guadano-Ferraz et al., 1997; Kohrle et al., 1990; Luna et al., 1995). Dio1 and Dio2 remove 5′ iodine from the outer tyrosine ring of T4 to produce T3 (Kohrle, 2000). Dio3, however, converts T3 and T4 to their inactive forms, rT2 and rT3, respectively, by deiodinating the inner tyrosine ring (Kohrle, 2000). All deiodinases share a conserved structural organization of alpha–beta–alpha (αβα) motifs (Callebaut et al., 2003).

A number of protein coding genes in *D. discoideum* genome share high identity to genes in the human genome (Eichinger et al., 2005; Harris et al., 2002; Langenick et al., 2008; Lee et al., 1998; Myre et al., 2011; Wessels et al., 2006). One among them is the type-III thyroxine 5′ deiodinase (*dio3*) gene (DDB_G0275741; www.dictybase.org; Lobanov et al., 2007). As the existence of thyroxine is not reported in *D. discoideum*, it is possible that Dio3 may be involved in deiodination of thyroxine or any unknown molecule. *dio3* is expressed both during growth and development. In slugs, *dio3* expression is confined to the prespore region. To understand the role of thyroxine 5′ deiodinase in *D. discoideum*, we generated *dio3* null cells (*dio3⁻*) by targeted gene disruption and studied the phenotype of *dio3⁻* in detail. Our data demonstrate that Dio3 is involved in aggregation, cell streaming and cell-type differentiation. Phototaxis of *dio3⁻* slugs is also impaired. qRT-PCR analyses of *acaA*, *carA*, *pdsA*, *regA*, and *pde4*, and Western blotting of CsaA and CadA suggest a prominent role for Dio3 in cAMP synthesis, relay and cell–cell adhesion.

Materials and methods

Bioinformatics analyses

Homologs of Dio3 were identified from the NCBI database using *D. discoideum* Dio3 as a query sequence. Dio3 sequences of various organisms were retrieved from the Dictybase (www.dictybase.org) and NCBI database. The Dio3 sequence of *D. discoideum* was used for online pBLAST (http://blast.ncbi.nlm.nih.gov/Blast.cgi), SMART (http://smart.embl-heidelberg.de/; Schultz et al., 1998) and PROF (https://www.predictprotein.org/; Rost et al., 2004) analyses. For sequence alignments, ClustalX (Jeanmougin et al., 1998) was used.

Dictyostelium culture and development

D. discoideum (Ax2) cells were grown in modified maltose-HL5 medium (28.4 g bacteriological peptone, 15 g yeast extract, 18 g maltose monohydrate, 0.641 g Na$_2$HPO$_4$ and 0.49 g KH$_2$PO$_4$ per litre, pH 6.4) containing 100 units penicillin and 100 μg/ml streptomycin-sulphate (HiMedia). Cultures were grown either as monolayers in Petri dishes or as shaking cultures (Erlenmeyer flask, Schott Duran) at a density of 2×10^6–4×10^6 cells/ml (150 rpm, 22 °C). Cells were allowed to develop after washing twice with KK2 buffer (2.25 g KH$_2$PO$_4$ and 0.67 g K$_2$HPO$_4$ in one litre water, pH 6.4) and were plated on non-nutrient agar plates (KK2 buffer, 15 g agar per litre, pH 6.4) at a density of 5×10^5 cells/cm^2.

Growth assays

Axenic growth was assayed as described by Jaiswal et al. (2012). Maltose-HL5 (25 ml) medium was used for growth and the initial cell density was adjusted to 1×10^5 cells/ml (22 °C, 150 rpm). Cell numbers were counted every 24 h, using a haemocytometer. For growth assays on bacteria, approximately 25 cells were deposited on *Klebsiella aerogenes* lawns, incubated at 22 °C and growth plaques were examined after 48 h and 72 h. The experiments were repeated four times in triplicates.

Generation of dio3 knockout

The *dio3* KO vector was engineered following the standard cloning procedures using pBluescript KSII+vector (Stratagene). Fragments from the 5′ and 3′ regions of *dio3* were PCR amplified using FP5′, RP5′ and FP3′, RP3′ primer pairs (Table S1), respectively and cloned in pTZ57r/t TA vector (Fermentas K1214). Both the 5′ and 3′ fragments were sub-cloned in pBluescript KSII+vector. Using the *XmaI* restriction enzyme, the blasticidin resistance (*bsR*) cassette was excised out of the pLPBLP vector (Faix et al., 2004) and ligated in between 5′ and 3′ arms of the *dio3* KO vector. Prior to transfection, we carried out restriction endonuclease digestion and DNA sequencing of the vector to confirm its integrity. Axenically grown Ax2 cells were washed twice with ice cold electroporation buffer (EP buffer: 10 mM K$_2$HPO$_4$, 10 mM KH$_2$PO$_4$ and 50 mM sucrose) and 1×10^7 cells were resuspended in 100 μl EP++ buffer (EP buffer+1 mM MgSO$_4$, 1 mM NaHCO$_3$, 1 mM ATP and 1 μM CaCl$_2$) containing 10 μg of linearized *dio3* KO vector. The cell suspension mixed with the linearized KO vector was transferred to pre-chilled cuvettes (2 mm gap, Bio-Rad) and electroporated (300 V, 2 ms, 5 square wave pulses with 5 s intervals) using a BTX ECM830 electroporator (Harvard Apparatus). Subsequently, the cell suspension was transferred to Petri dish containing 10 ml HL5 medium and incubated at 22 °C. After 24 h, the cultures were replaced with fresh HL5 supplemented with 10 μg/ml blasticidin (MP Biomedicals). Blasticidin resistant clones were isolated after three days, mixed with autoclaved *K. aerogenes* and plated on SM5 agar plates containing 10 μg/ml blasticidin and incubated at 22 °C. To confirm *dio3* disruption, the genomic DNA of several recombinant clones was subjected to PCR analyses using different primer combinations (Table S1; Supplementary information). Four independent *dio3⁻* clones were obtained and one of them was used for further studies. *dio3* gene disruption was also confirmed by Southern hybridization. The *bsR* fragment from pLPBLP and the 5′ arm of *dio3* KO vector were excised, gel purified, and DIG labeled as described by the manufacturer (Roche) and used as probes for Southern hybridization.

Construction of Dio3 reporter fusion and expression vectors

Using genomic DNA as a template, we PCR amplified a 749 bp fragment 5′ upstream of *dio3*, including the sequence coding for the first 13 amino acids of Dio3 and ligated the amplicon in a pTX-GFP vector by exploiting the *SalI* and *KpnI* restriction sites. The resulting vector pdio3promoter::GFP had GFP along with 13 amino acids of Dio3, under the control of *dio3* promoter sequence. This vector was electroporated to Ax2 cells and the GFP expressing clones were selected in the presence of 10 μg/ml G418 as described above.

For generating the Dio3 expression vector carrying N-terminal GFP tags, we PCR amplified 771 bp of *dio3* gene along with the 3′ UTR (393 bp) containing the selenocysteine insertion sequences, SECIS (109 bp). Both the PCR amplified DNA fragment and pTX-GFP vector were digested with *SacI/XhoI* restriction enzymes, purified with Qiagen PCR purification kit and subjected to ligation. The

resulting vector will thus code for Dio3 with N-terminal GFP tag synthesized under actin 15 promoter. The pTX-GFP::*dio3* vector was transfected to Ax2 and *dio3*⁻ cells and the transformants were selected in the presence of 10 μg/ml G418. The GFP::Dio3 fusion protein expression was confirmed by Western blotting using anti-GFP antibodies (Santa Cruz Biotechnology). Primer sequences used for generating the vectors are mentioned in Table S2.

Microscopy

A Nikon SMZ-1000 stereo zoom microscope with epifluorescence optics or a Nikon 80i Eclipse upright microscope equipped with a digital sight DS-5MC camera (Nikon) was used for microscopy. Images were processed with NIS-Elements D (Nikon) or Image J.

GFP/RFP reporter constructs

Ax2 and *dio3*⁻ strains were transformed with prestalk and prespore cell-type specific markers *ecmA*-GFP (Good and Kuspa, 2000), *pspA*-RFP (Parkinson et al., 2009) (a kind gift from Christopher Thompson, University of Manchester, UK), and pTX-GFP (Levi et al., 2000) plasmids, as described above. The transformants were selected with 10 μg/ml G418 as described above.

Western blotting

To examine the expression levels of CsaA, CadA, GFP and actin, we grew Ax2 and *dio3*⁻ cells in HL5 medium, washed twice with KK2 buffer and 5×10^5 cells/cm² were developed on 0.45 μm nitrocellulose membranes at 22 °C. Cells were harvested at the indicated time points, lysed with 200 μl lysis buffer (2% SDS, 0.5 M Tris, pH 6.8) containing 1% mercaptoethanol and boiled for 5 min (Jaiswal et al., 2012). Protein concentration was determined by the Bradford assay (Bio-Rad). Cell lysates were analyzed by electrophoresis in 10–12% polyacrylamide gels and were blotted onto a nitrocellulose membrane (Bio-Rad). The membranes were independently incubated with anti-CsaA (Bertholdt et al., 1985; Ochiai et al., 1982) (1:10; a kind gift from Ludwig Eichinger, University of Cologne, Germany), anti-CadA (Knecht et al., 1987) (1:10,000; a kind gift from Chi-Hung Siu, University of Toronto, Canada), anti-GFP (Mitra et al., 2003) (1:5000; Santa Cruz Biotechnology) and anti-actin (Simpson et al., 1984) (1:10; a kind gift from Angelika Noegel, University of Cologne, Germany) primary antibodies overnight at 4 °C. Membranes were washed thrice with TBST buffer (50 mM Tris–HCl, pH 7.4, 150 mM NaCl and 0.1% Tween 20) for 30 min and thereafter, the membranes were incubated with secondary antibodies (1:4000) conjugated with horseradish peroxidase (HRP) for 1 h at RT. Subsequently, the membranes were washed and developed using ECL kit (GE Healthcare). Actin was used as a loading control. Western blotting was carried out thrice and images were quantified using ImageJ and normalized to actin expression levels.

Semi-quantitative reverse transcription PCR (RT-PCR) and quantitative real time PCR (qRT-PCR)

For quantitative RT-PCR, Ax2 and *dio3*⁻ cells were developed on 0.45 μm nitrocellulose membranes and total RNA was isolated at the indicated time points (0–24 h) using RNAeasy kit (Qiagen). RNA samples were quantified with a spectrophotometer (Eppendorf) and were also analyzed on 1% TAE agarose gels. cDNA was synthesized from total RNA using a cDNA synthesis kit (Applied Biosystems). 3 μg of RNA was used as template to synthesize cDNA using random primers provided by the manufacturer. 1 μl of cDNA was used for qRT-PCR, using SYBR Green Master Mix (Thermoscientific). qRT-PCR was carried out to analyze the transcription levels of *dio3* (0–24 h), *acaA carA*, *pdsA*, *regA* (0–12 h) and *pde4* (4–20 h) using the Eppendorf Mastercycler Realplex[4]. Semi-quantitative RT-PCR was carried out with Ax2 and *dio3*⁻ cDNA to analyze the expression levels of *ecmA* and *pspA* genes at the indicated time points. *rnlA* was used as a control. The primer sequences are mentioned in Tables S3 and S4. All the qRT-PCR data were analyzed as described by Schmittgen and Livak (2008). RT-PCR and qRT-PCR were carried out thrice and RT-PCR images were quantified using Image J.

cAMP quantification

cAMP quantification was performed using the cAMP-XP™ assay kit as per the manufacturer's protocol (Cell Signaling, USA). Ax2 and *dio3*⁻ cells were developed on 0.45 μm nitrocellulose membrane (Millipore) for 8 h, lysed with 100 μl of 1X lysis buffer and incubated on ice for 10 min. 50 μl of lysed sample and 50 μl HRP conjugated cAMP solution were added to the assay plate, incubated at RT on a horizontal orbital shaker. After 3 h, the wells were emptied, washed thrice with 200 μl of 1X wash buffer, then 100 μl of tetra-methylbenzidine (TMB) substrate was added and incubated at RT for 10 min. The reaction was terminated by adding 100 μl of stop solution and the absorbance was measured at an optical density (OD) of 450 nm. cAMP standard curve was used to calculate absolute cAMP levels in *D. discoideum*. The values represent the average of three independent experiments.

Chemotaxis assay

We carried out under-agarose assay to monitor *D. discoideum* chemotaxis towards 0.1 mM folate (Laevsky and Knecht, 2001). Cell migration was recorded for 5 min at 10 s intervals using a Nikon inverted (TE 2000) microscope, under a 20 × objective. The movies of migrating cells were analyzed as described by Blagg et al. (2003). The average speed of 21 migrating cells from each experiment was determined using ImageJ MTrackJ software. Three independent assays were carried out to ascertain chemotaxis defect in *dio3*⁻.

Qualitative slug phototaxis assay

Qualitative phototaxis assays were performed according to modified protocols of Flegel et al. (2011) and Fisher and Annesley (2006). Ax2 and *dio3*⁻ cells were grown to mid-log phase in maltose-HL5 medium and washed thrice with ice-cold developmental buffer (DB: 5 mMNa₂HPO₄, 5 mM KH₂PO₄, 1 mM CaCl₂, 2 mM MgCl₂, pH 6.5). After adjusting the cell density to 5×10^8 cells/ml, 10 μl of the cell suspension was spotted on DB-agar plates containing 1.5% agar and 0.5% activated charcoal to reduce stray light. Plates were covered with black paper and aluminum foil with a small hole (approx. 1–2 mm) on the opposite side of the cell droplet. Control plates were covered completely. Plates were incubated at 22 °C under a light source for 2–3 days. Later, the plates were uncovered; cells, slugs and slime trails were transferred for 2 h on a white nitrocellulose membrane (Protran BA85, Schleicher and Schuell). The membranes were stained with 0.1% amido black for 10 min. Membranes were destained with 30% acetic acid and 10% methanol in double distilled H₂O for 10–15 min, rinsed with water, and air-dried. Finally, stained cellular structures and slime trails were scanned. The phototaxis assays were repeated thrice.

Cell–cell adhesion assay

Cell–cell adhesion assays were performed as described by Desbarats et al. (1994). Cells growing at mid-log phase were harvested, washed twice with Sörensen's buffer (SB), cell density was adjusted to 3×10^6 cells/ml in SB and starved at 22 °C in an orbital shaker set to

150 rpm. At the time points indicated, 500 µl of cell suspensions were transferred to 1.5 ml microcentrifuge tubes, vortexed for 20 s, and mixed thoroughly for 20 min using a rotator shaker (Tarsons). 10 µl aliquots were used to count single cells and cells bound to each other or cell clumps were ignored. Experiments were performed in triplicates and were repeated thrice. The mean values obtained for single cells were used to calculate the cell–cell adhesion percentage.

To measure the EDTA-resistant cell–cell adhesion, mid log phase cells were harvested, washed twice with SB, resuspended in KK2 buffer at a density of 1×10^7 cells/ml and starved in the presence or absence of 5 mM EDTA at 180 rpm on a platform shaker. 10 µl cell suspension was taken at the indicated time points to count single cells; cells bound to each other or cell clumps were ignored. Three independent experiments were performed in triplicate and the mean values obtained for single cells were used to calculate the cell–cell adhesion percentage.

Statistical tools

Microsoft Excel (2007) was used for data analyses. Unpaired Student's *t*-test (GraphPad Prism, version 6) was used to determine the statistical significance.

Results

Sequence analyses of D. discoideum Dio3

dio3 is an intronless gene in *D. discoideum*, present in chromosome II and codes for a protein of 257 amino acids with selenocysteine at position 113 (www.dictybase.org; Lobanov et al., 2007). Human Dio3 is 304 amino acids long with a selenocysteine residue in its active site (Salvatore et al., 1995). The active site region is highly conserved in these two species (red box; Fig. 1A, pink circle represents selenocysteine). *D. discoideum* Dio3 shares 37% identity with human Dio3 and the pBLAST analysis suggested that Dio3 belongs to the thioredoxin-like superfamily (Fig. S1A). Pfam search using the online SMART tool (http://smart.embl-heidelberg.de/) predicted a T4-deiodinase domain within the Dio3 of *D. discoideum* with a high degree of confidence (7.1e–44; Fig. S1B). Therefore, it is likely that this Dio3 could be an orthologue of human type III deiodinase.

Dio3 is also present in other slime molds such as *Dictyostelium purpureum*, *Dictyostelium fasciculatum* and *Polysphondylium pallidum*, but in these it lacks the selenocysteine residue. Amino acid sequences of slime molds Dio3 and vertebrate Dio3 were aligned using ClustalX. Multiple sequence alignment of various vertebrates and slime molds Dio3 amino acid sequences were used to create a phylogenetic tree employing BLOSUM62 of ClustalX alignment in JALVIEW version 2 (Waterhouse et al., 2009). Our analyses suggest that *D. discoideum* Dio3 falls in a separate clade and is a distant relative of vertebrate homologs (Fig. 1B).

Using the secondary structure prediction tool PROF (https://www.predictprotein.org/; Rost et al., 2004), we found that similar to human Dio3, *D. discoideum* Dio3 has αβα (α-blue blocks, β-red blocks) motifs in its secondary structure (Fig. S1C; Callebaut et al., 2003). However, unlike human Dio3, *D. discoideum* Dio3 lacks the membrane binding domain. Secondary structure prediction analyses suggest that Dio3 is conserved between social amoebae and vertebrates.

Dictyostelium synthesizes full length Dio3 protein in spite of an intermediate stop codon TGA

Dio3 contains a rare amino acid selenocysteine in its active site, which is encoded by a stop codon TGA. The Dictybase (www.dictybase.org) genome data also suggest that *D. discoideum* dio3

cDNA contains a TGA codon. The existence of a deiodinase like protein in *D. discoideum* has been reported earlier by metabolic labeling with [75]Se (Lobanov et al., 2007). To ascertain if *D. discoideum* synthesizes a full length Dio3 protein, we constructed an expression vector carrying N-terminal GFP tagged to Dio3. As a 3′ UTR is necessary to code TGA as a selenocysteine, a 393 bp of 3′ UTR of *dio3* was also engineered in the vector (Fig. 2A). GFP expression was observed throughout development (Fig. 2B). GFP::Dio3 fusion protein expression was confirmed by Western blotting, using anti-GFP antibody. The observed GFP band size was close to 27 kDa and the predicted size of the full length Dio3 was 30.5 kDa. As expected, we obtained the Dio3::GFP fusion protein of size 57.5 kDa. A band shift of approximately 30.5 kDa was observed between GFP and GFP::Dio3 in the Western blots (Fig. 2C). This observation confirms that *D. discoideum* synthesizes a full length Dio3. An additional band in the Ax2/GFP::Dio3 lane near the GFP band could be due to non-specific proteolytic cleavage of the fusion protein.

Constitutive expression of dio3 during growth and development

In vertebrates, thyroxine deiodinases are expressed in a tissue specific manner to regulate both growth and development. To examine if expression of *dio3* is developmentally regulated, we performed qRT-PCR from RNA isolated at different developmental stages. The time points tested included 0, 2, 4, 6, 9, 12, 16, and 24 h. We found that *dio3* was expressed throughout development but to a greater degree in later stages (Fig. 3).

Cell-type specific expression of dio3

qRT-PCR analyses suggested that *dio3* was expressed throughout growth and development, but expression was upregulated during mound, slug and fruiting body stages (Fig. 3). To confirm this expression pattern of *dio3*, the actin 15 promoter from pTX-GFP vector was replaced with the 5′ upstream region of *dio3* (749 bp) and was subsequently transfected to Ax2 cells. *dio3* promoter::GFP expression was analyzed by Western blotting. Corroborating the qRT-PCR results, *dio3* promoter expression was markedly high in the slug stage (Fig. 4A). Presumably, the 749 bp 5' upstream fragment of *dio3* serves as a promoter to drive *dio3* expression during *D. discoideum* development.

To examine the cell-type specific expression of *dio3*, we analyzed the expression pattern of GFP under the control of *dio3* promoter during growth and development. GFP expression was seen throughout growth and multicellular development and in the slug stage GFP expression was restricted to the posterior prespore region (Fig. 4B). GFP expression was also seen in the posterior regions of culminants and the spore masses of the fruiting bodies. The confined expression of GFP in the prespore region suggests that Dio3 may possibly be involved in patterning and spore differentiation.

dio3 disruption

The ubiquitous expression of *dio3* suggested that it could be involved in development in *D. discoideum*. To investigate this possible role of Dio3, we generated a knockout by targeted gene disruption. Homologous recombination between the *dio3* knockout vector and the endogenous *dio3* removed 241 bp of the coding region and integrated the blasticidin resistance (*bsR*) cassette instead (Fig. S2A). Blasticidin resistant clones were selected and *dio3* disruption was confirmed by Southern hybridization and PCR analyses (Fig. S2B and C; Supplementary information). RT-PCR analyses showed that *dio3* mRNA expression was completely absent both during growth and development in *dio3*⁻ (Fig. S3).

A

D. discoideum
H. sapiens

D. discoideum
H. sapiens

D. discoideum
H. sapiens
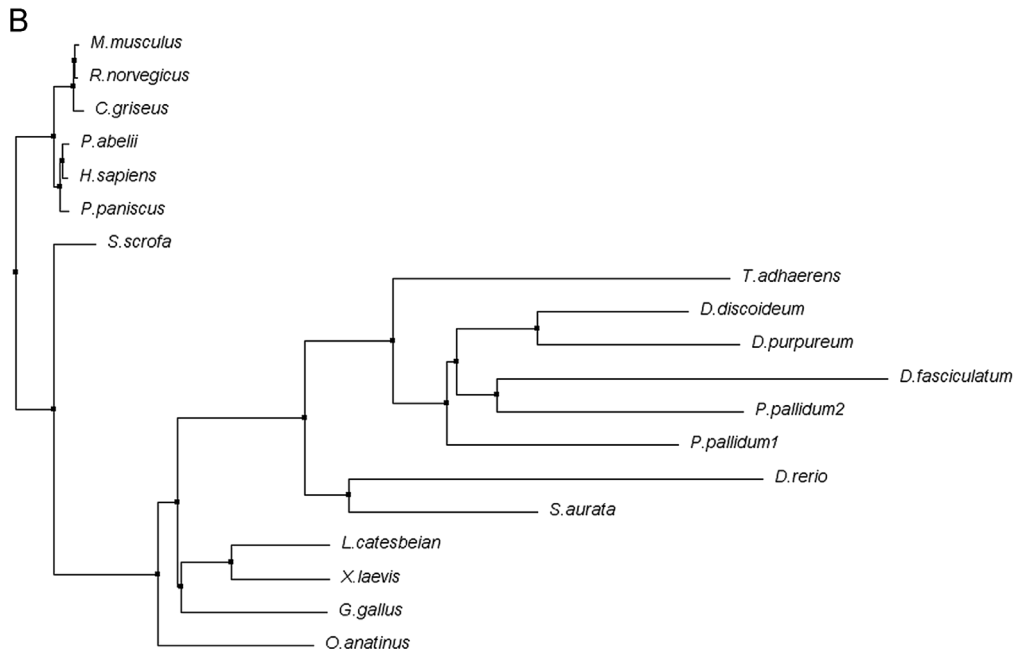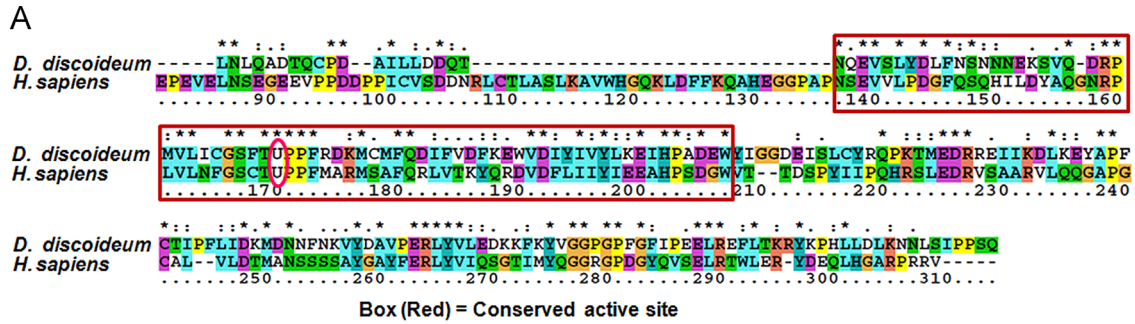
Box (Red) = Conserved active site

B

Fig. 1. Dio3 amino acid sequence alignment and phylogenetic analysis. (A) Amino acid sequence alignment of Dio3 from *Homo sapiens* and *D. discoideum* determined with ClustalX. The conserved active site region of Dio3 is highlighted in the red rectangle and the pink circle represents the presence of selenocysteine (U) in the active site. (B) A phylogenetic tree showing the relationship of *D. discoideum* Dio3 with Dio3 from other organisms. The Neighbor Joining Tree was constructed using BLOSUM62 of a ClustalX alignment in JALVIEW.

A

B

C
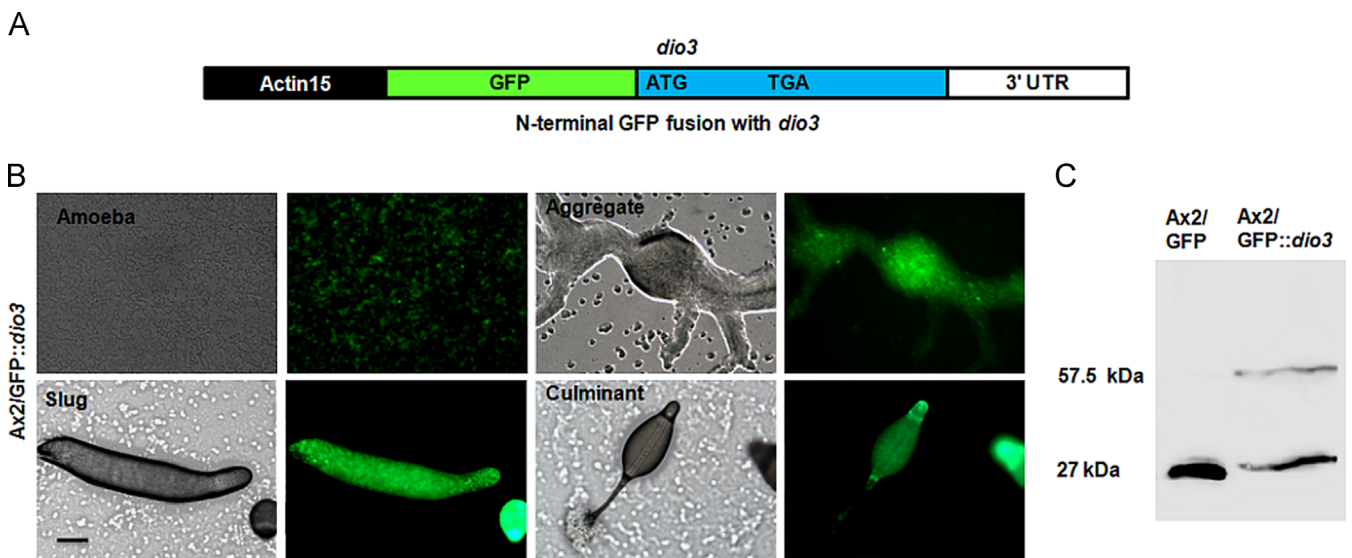
Fig. 2. Expression of Dio3 protein in *D. discoideum*. (A) A schematic representation of generation of the Dio3 expression vector. The ORF of Dio3 containing the 3′ UTR sequence (1167 bp) was PCR amplified and cloned in a pTX–GFP vector downstream of GFP by maintaining the reading frame. The resultant vector was transfected to Ax2 cells. (B) GFP expression in different developmental stages. Scale bar=200 µm. (C) Confirmation of full length Dio3 synthesis. Protein samples from Ax2 cells expressing GFP::Dio3 were prepared and used for Western blotting using anti-GFP antibody. A band corresponding to the molecular weight of the fusion protein ($\sim$57.5 kDa) is indicated. The presence of an additional band near GFP could be possibly due to non-specific proteolytic cleavage of the GFP::Dio3 fusion protein.

Growth kinetics of dio3⁻ in axenic cultures and on bacterial plates

Dio3 is known to regulate growth in vertebrates (Orozco et al., 2012) but its function in *D. discoideum* is unknown. To monitor the growth rate of *dio3⁻* cells in axenic conditions, the initial cell density was adjusted to 1×10^5 cells/ml and thereafter the cell
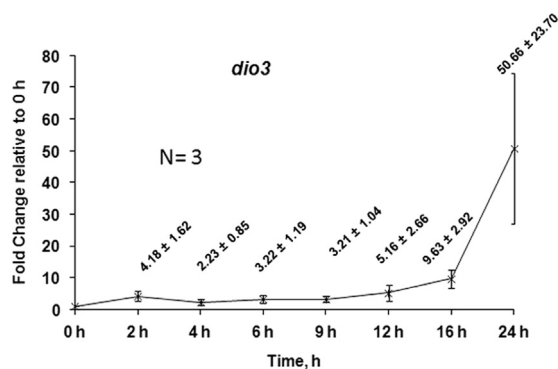

Fig. 3. Transcriptional regulation of *dio3* during growth and development of *D. discoideum*. qRT-PCR analysis of *dio3*-mRNA at different time points in parental Ax2 cells. *dio3* expression at various time points was determined relative to the expression at the vegetative state (0 h) of *D. discoideum*. *rnlA* was used as a control. qRT-PCR was carried out thrice. Error bars represent the mean and standard deviations. Primer sequences are mentioned in Table S3.

number was periodically monitored. *dio3⁻* cells had a longer doubling time than Ax2 cells in HL5 medium (Fig. 5A). The average doubling time of *dio3⁻* was 14 h but Ax2 had a doubling time of 12 h. Further, we tested the growth of *dio3⁻* on *K. aerogenes* lawns and analyzed the size of phagocytic plaques formed. The growth plaques formed by *dio3⁻* were significantly smaller than those formed by Ax2. By 48 h, Ax2 cells formed plaques and by 72 h, they had exhausted the bacterial lawn, undergone development and formed slugs. Conversely, in *dio3⁻* after 48 h small plaques were observed and even after 72 h, only aggregates could be seen (Fig. 5B). Compared to Ax2, *dio3⁻* formed small plaques (Fig. 5C). The complemented strain, *dio3⁻* [*act15/gfp::dio3*], showed rescue in the growth defect (Fig. 5A). These observations strongly imply that Dio3 is required for both axenic and xenic growth of *D. discoideum*.

Formation of multiple aggregation centers during late aggregation in dio3⁻

We studied the development of *dio3⁻* on non-nutrient KK2 agar after plating them at a density of 5×10^5 cells/cm². When compared with Ax2, *dio3⁻* formed aggregates with longer streams after 4 h delay (Fig. 6A) and similar results were observed even in submerged conditions on a plastic surface (Fig. S4). The number of aggregates formed by Ax2 and *dio3⁻* were 13 ± 0.7, 6.3 ± 0.4 aggregates/cm², respectively (Fig. 6B, $p < 0.01$). A striking phenotype of *dio3⁻* is the
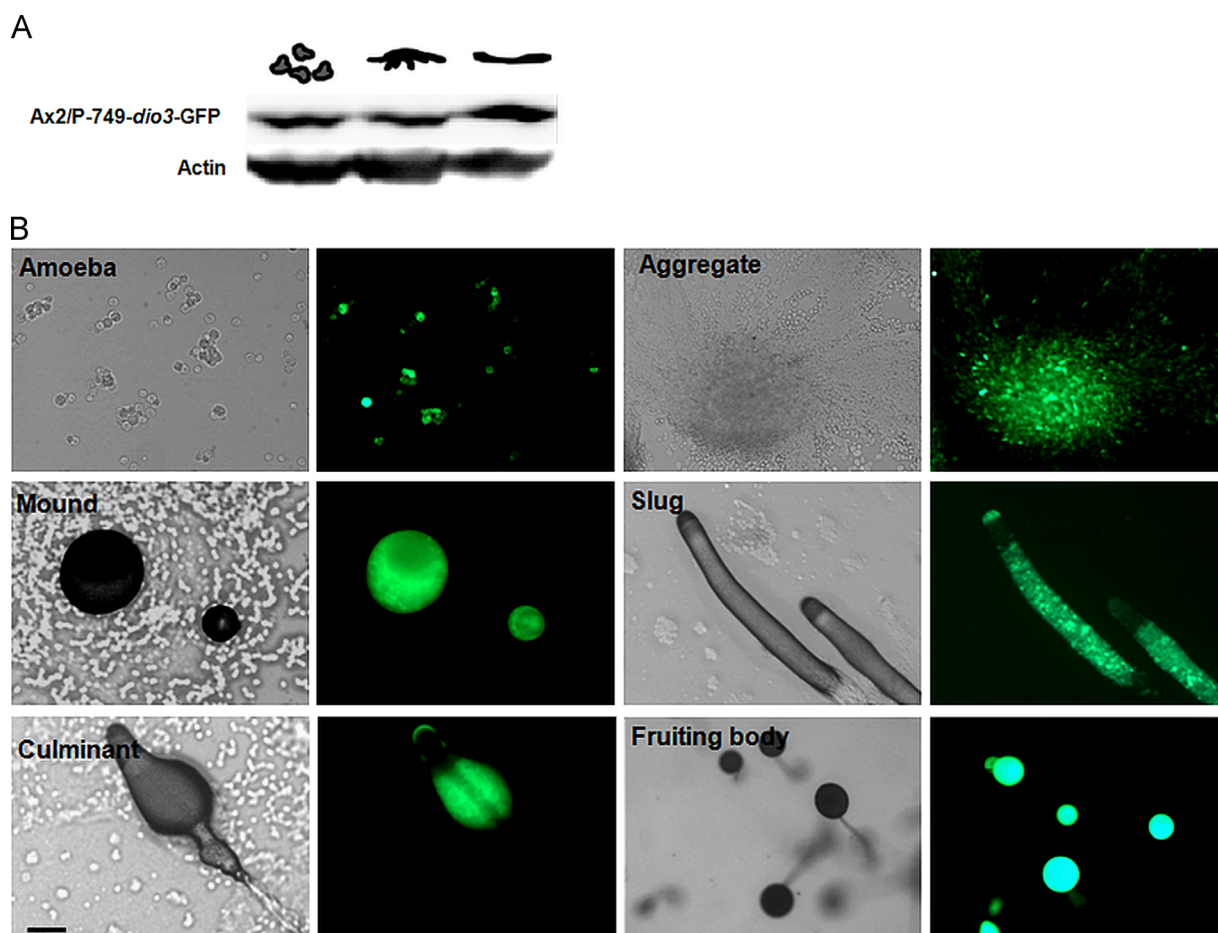

Fig. 4. *dio3* promoter-GFP expression. (A) *dio3* promoter (749 bp) activity in amoebae, aggregate and slug. Ax2 cells transformed with the *dio3* promoter::GFP construct were allowed to develop on non-nutrient KK2 agar plates. Protein samples were prepared from amoebae, aggregates and slugs were used for Western blot analyses, with an anti-GFP antibody. (B) *Dio3* promoter::GFP expression in various developmental stages of Ax2. GFP expression is restricted in the prespore region of slug. Scale bar=200 μm.
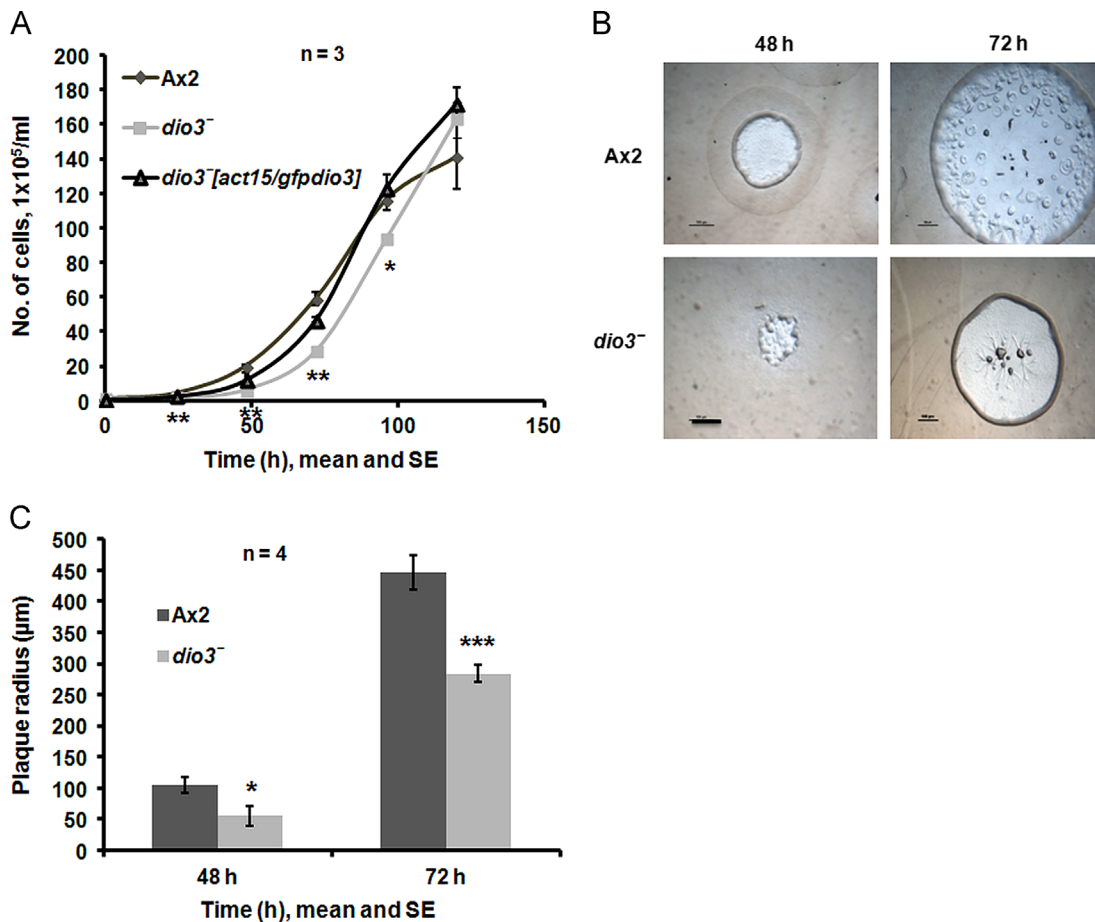
Fig. 5. Growth kinetics and plaque formation assay. (A) Growth rate of *D. discoideum* Ax2, *dio3⁻* and *dio3⁻* [*act15/gfp::dio3*] cells. The initial cell number was 1×10^5 cells/ml and thereafter the growth kinetics were monitored for 5 days. The *X* and *Y* axes represent the cell counting time points and the corresponding number of cells, respectively. The error bar represents the mean and standard error ($n=3$). (B) Plaques formed by Ax2 and *dio3⁻* on *K. aerogenes*. Scale bar$=100$ μm. (C) Measurement of plaque radius for Ax2 and *dio3⁻* cells. The plaque radius of 12 plaques in each experiment was measured using the NIS-Element D software. Mean and standard error are represented. Data shown here represents the average of three or more independent experiments ($*p < 0.05$, $**p < 0.01$, $***p < 0.001$).

formation of small protrusions along the cell streams during late aggregation (arrow); later these break into small mounds and form fruiting bodies (Fig. 6A; Supplementary Videos 1 and 2). Due to uneven fragmentation, the mounds, culminants and fruiting bodies formed by *dio3⁻* were heterogeneous in size. To examine the integrity of *dio3⁻* aggregates at a higher cell density, 1×10^6 cells/cm² were plated and we observed a similar 'stream breaking' phenotype (Fig. S5). When *dio3⁻* cells were reconstituted with Ax2 in a 9:1 ratio, the developmental defects (large aggregates, stream breaking) were rescued in the *dio3⁻*:Ax2 chimeras (Fig. 6C). The complemented strain, *dio3⁻* [*act15/gfp::dio3*], showed rescue in the developmental phenotype of *dio3⁻* (Fig. 6A and B; Supplementary Video 2A). Our results strongly imply that Dio3 is required for the integrity of late aggregates and for further transition to later morphogenetic stages.

Supplementary material related to this article can be found online at http://dx.doi.org/10.1016/j.ydbio.2014.10.012.

Impaired chemotaxis and phototaxis

The smaller plaques formed by *dio3⁻* on bacterial lawns indicated that cell movement may be impaired. Therefore, we tested the chemotactic ability of *dio3⁻* towards folate under a thin layer of agarose. Ax2 cells were elongated and showed several protrusions towards folate. Even though *dio3⁻* cells formed protrusions towards folate, they were smaller than those seen in Ax2 cells (Videos S3 and S4). The speed at which the cells migrated towards folate was determined using ImageJ (Fig. 7). *dio3⁻* cells moved randomly but at

a slower pace compared to Ax2. The average speed of *dio3⁻* was 14.4 ± 0.4 μm/min, whereas Ax2 cells moved towards the folate at 18.2 ± 1.1 μm/min. The decreased speed of *dio3⁻* cells might also account for small plaques formed on the bacterial lawns. The folate chemotaxis defect of *dio3⁻* was rescued in the complemented strain, *dio3⁻* [*act15/gfp::dio3*] (Fig. 7; Supplementary Video 5). These results suggest that Dio3 is important for normal cell movement.

Supplementary material related to this article can be found online at http://dx.doi.org/10.1016/j.ydbio.2014.10.012.

The slug tip of *D. discoideum* is known to be sensitive to heat and light (Fisher, 2001). To determine the role of Dio3 in slug phototaxis, qualitative assays were carried out. As shown in Fig. 8, *dio3⁻* formed fewer and smaller slugs, which showed no general defect in phototaxis but the migration speed of the slugs was slower than that of Ax2 slugs. In the time it took for Ax2 slugs to move across the plate towards the light source, the *dio3⁻* slugs moved only 75% of the distance. The observed difference in phototactic behavior of *dio3⁻* suggests that Dio3 could also be involved in photodetection.

Weak cAMP relay and defective cell–cell adhesion: possible causes of long cell streams, stream breaking and delayed development in dio3⁻

The late aggregates of *dio3⁻* had many signaling centers, suggesting defects in cAMP synthesis and relay. To test this notion, we first performed an ELISA-based photometric assay to quantify cAMP levels. After 8 h of development, the estimated cAMP levels were 12.1 ± 2.5 nM and 2.7 ± 0.3 nM in Ax2 and *dio3⁻*, respectively
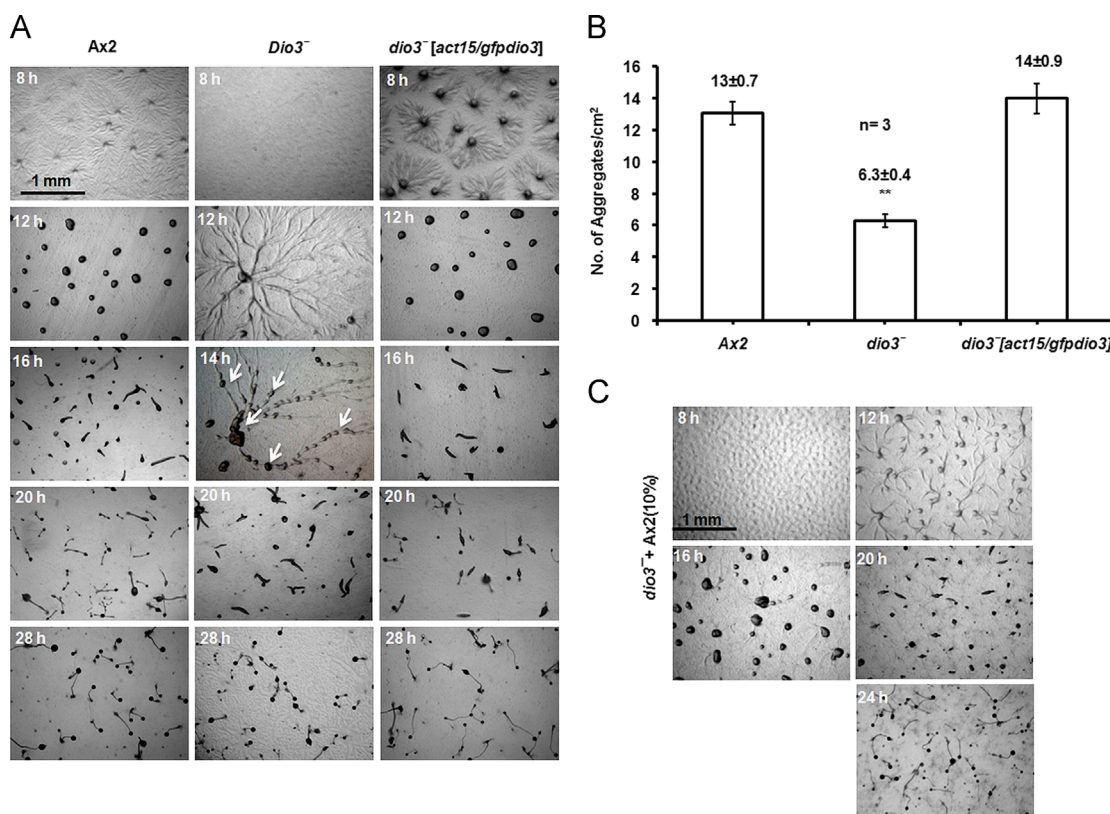
Fig. 6. Developmental phenotype of *dio3⁻*. (A) Phenotype of parental Ax2, *dio3⁻* and *dio3⁻* [*act15/gfp::dio3*] cells. *dio3⁻* formed aggregates after a 4 h delay. Multiple signaling centers in the aggregation streams of *dio3⁻* by 14 h (white arrow). For observations, the cells were plated at a density of 5×10^5 cells/cm², followed by incubation at 22 °C. Scale bar=1 mm. (B) Quantitative measurements of aggregation. The number of aggregates was counted in a centimeter square area. (C) Phenotype of *dio3⁻* was rescued by mixing with 10% Ax2 cells. The experiments were repeated thrice ($p < 0.01$).
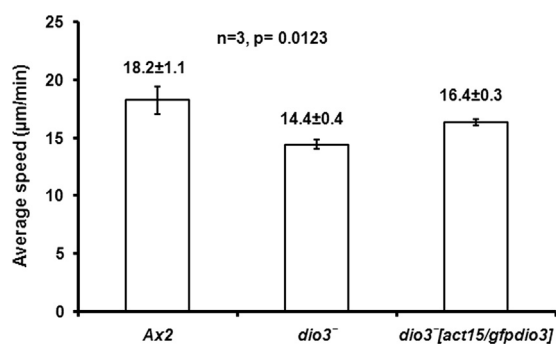

Fig. 7. Chemotaxis speed of Ax2, *dio3⁻* and *dio3⁻*[*act15/gfp::dio3*] cells. The average cell speed was determined by calculating the distance moved in 5 min. This graph represents the mean and standard deviation of 3 independent experiments where the average speed of 21 cells was calculated in each experiment ($p=0.0123$).

(Fig. 9A, $p=0.0048$). However, the light scattering (Lusche et al., 2004) data showed that the *dio3⁻* cells still respond to cAMP and also show autonomous oscillations (Fig. S6).

We further examined the expression of the candidate genes involved in cAMP synthesis and relay by qRT-PCR. In *dio3⁻*, *acaA* expression was down regulated by 16.4 ± 4.2 fold at 4 h and 2.7 ± 0.4 fold at 6 h of development (Fig. 9B). Similarly, *carA* expression in *dio3⁻* was also reduced by 7.2 ± 1.1 fold at 4 h and 1.0 ± 0.3 fold at 6 h of development when compared with Ax2 (Fig. 9C). We observed 3–4 fold reduction in relative mRNA expression levels of cAMP phosphodiesterases (*pdsA* and *regA*) at 2–6 h; but at 9 h and 12 h the expression levels were high in *dio3⁻* (Fig. 9D and E). *pde4* expression, however, was low at 4–9 h of development in *dio3⁻* (Fig. 9F). These results imply that cAMP
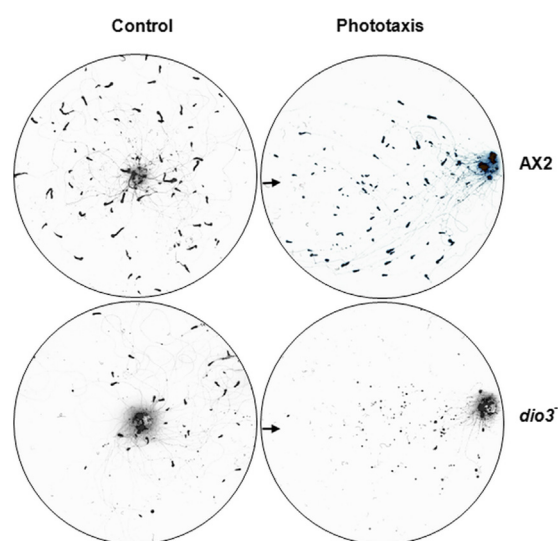

Fig. 8. Phototaxis assay of Ax2 and *dio3⁻* cells on DB-charcoal-agar. Plates were kept for 3 days under a light source as explained in *Materials and methods*. Arrows indicate the side of the hole/light source. A droplet of cells was deposited in the center on control plates, covered and kept in total darkness. Images of Ax2 and *dio3⁻* slugs moving towards a light source are shown. This experiment was repeated thrice.

synthesis and relay are affected in *dio3⁻*, which might account for delayed development and stream breaking.

Cell–cell adhesion is another feature of *D. discoideum* development that is highly augmented by the cAMP relay. We therefore assayed cell–cell adhesion and quantified the expression levels of
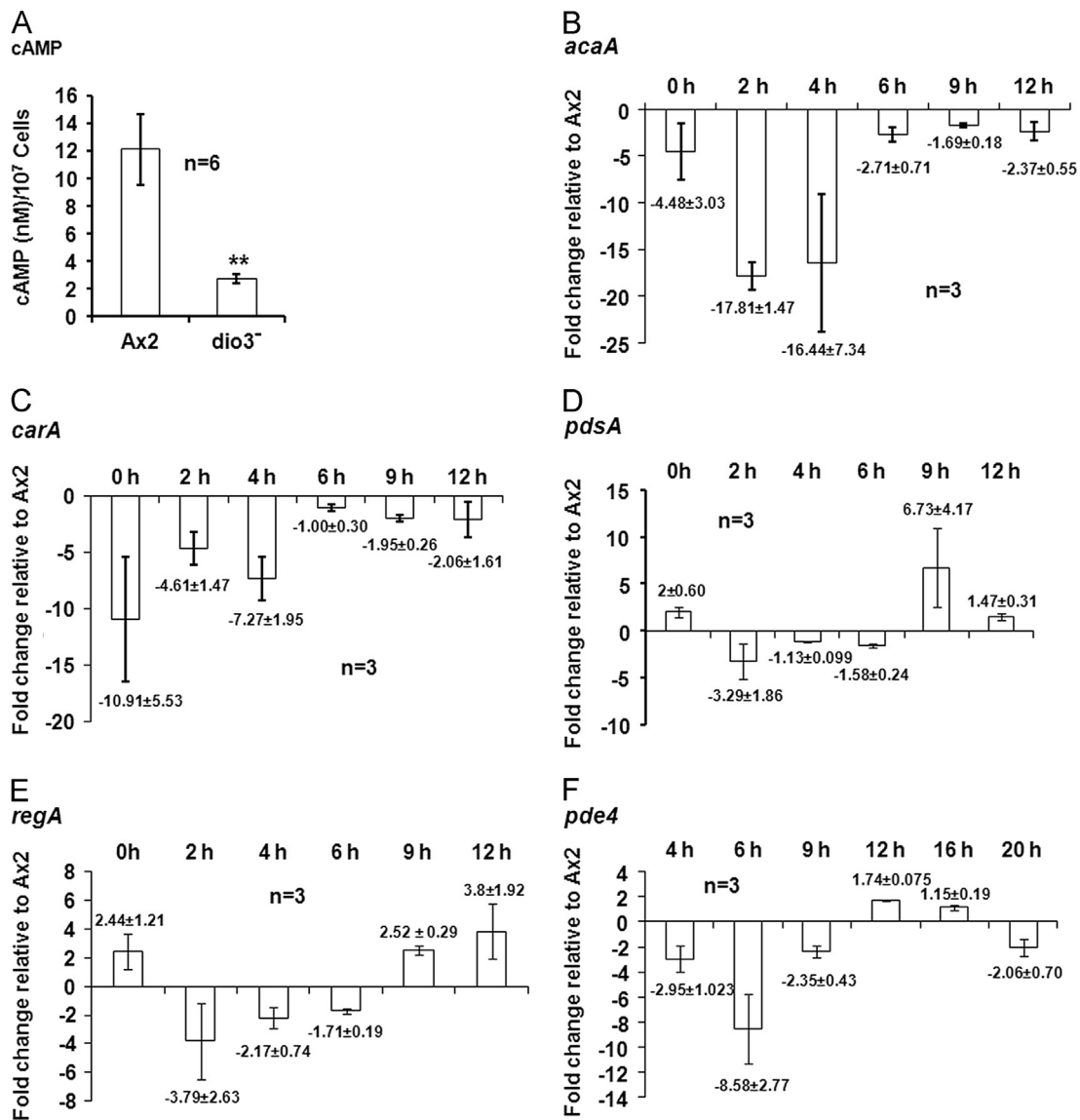
Fig. 9. cAMP relay and expression of *acaA*, *carA*, *pdsA*, *regA* and *pde4* in *dio3⁻*. (A) cAMP levels at 8 h of development in Ax2 and *dio3⁻* ($p=0.0048$, $n=6$). (B) Down regulation of genes involved in cAMP relay in *dio3⁻* – *acaA*, (C) *carA*, (D) *pdsA*, (E) *regA*, and (F) *pde4*. Fold change in mRNA expression is relative to Ax2 at the indicated time points. Primer sequences are listed in Table S3. *rnlA* was used as a control. The experiments were repeated thrice ($n=3$).

CadA and CsaA, which normally begin during aggregation. We observed 40–50% reduction of cell–cell adhesion in *dio3⁻* cells (Fig. 10A) and EDTA sensitive cell adhesion was also affected (Fig. 10B). As aggregate formation in *dio3⁻* was delayed (by 4 h, see Fig. 6A), CsaA expression was also delayed. While CsaA expression was observed after 4 h of development in Ax2, it only started at 9 h in *dio3⁻* (Fig. 10C, Table S5). A significant decrease in CadA expression in *dio3⁻* was also observed during early development compared with Ax2 (0–12 h; Fig. 10C, Table S6). The altered levels and timings of CadA and CsaA expression could possibly cause the cell–cell adhesion defect. This impaired cell–cell adhesion might account for delayed aggregation and stream breaking in *dio3⁻*.

Altered cell fates and cell-type proportions in dio3⁻ slugs

To examine if cell-type proportions were altered in *dio3⁻*, we examined the expression patterns of prestalk (*ecmA*) and prespore (*pspA*) markers in the *dio3⁻* slug (Fig. 11A). In *dio3⁻* slugs, the *ecmA*-GFP region was enlarged compared with Ax2 slugs. If the entire slug length is considered 100%, *ecmA*-GFP reporter spans an average of $21.2 \pm 2.1\%$ in Ax2 slugs and $30.8 \pm 3.9\%$ in *dio3⁻* slugs ($p=0.0015$).

Similarly, we also found a difference in *pspA*-RFP expression between Ax2 and *dio3⁻* slugs. The *pspA*-RFP regions were $76.1 \pm 3.6\%$ in Ax2 and $67.4 \pm 2.9\%$ in *dio3⁻* ($p=0.0031$). Our RT-PCR analyses corroborated these observations as *ecmA* expression was high and *pspA* levels were down regulated in *dio3⁻* (Fig. 11B and C).

To examine the cell fate preferences of *dio3⁻* in chimeric slug, either Ax2 or *dio3⁻* cells were marked with GFP, and mixed in a 20:80 ratio and thereafter we tracked the cell fate of *dio3⁻* during development. In a chimeric slug of 20% *dio3⁻*-GFP and 80% unmarked Ax2, we observed *dio3⁻*-GFP cells predominantly occupying the prestalk region. However, in the chimeric slugs of 20% Ax2-GFP and 80% unmarked *dio3⁻*, Ax2-GFP cells were confined to the prespore region (Fig. 12). Our reconstitution studies imply that *dio3⁻* cells have the tendency to form prestalk cells and Dio3 is important for prespore differentiation.

Discussion

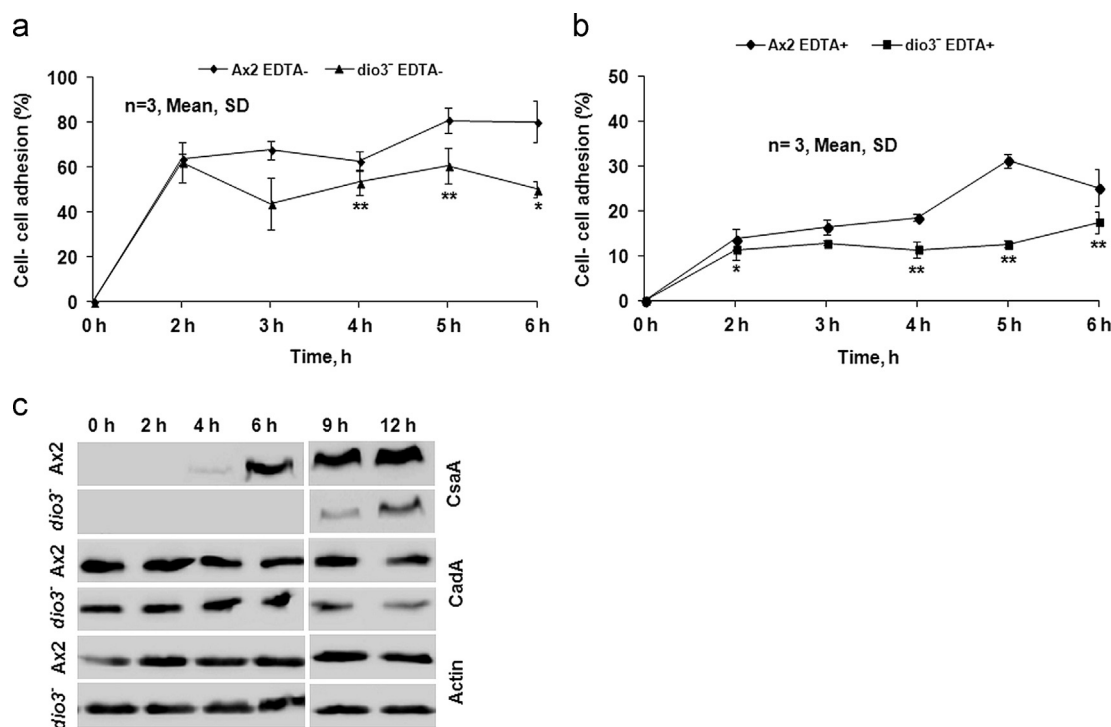Dio3 is present in many vertebrates, where it inactivates thyroxine hormones by deiodinating T3 and T4 (Kohrle, 2000)

Fig. 10. Cell–cell adhesion measurement and CsaA and CadA expression analyses during aggregation. (A) Impaired cell–cell adhesion in $dio3^-$ cells. By scoring the presence of single cells at the indicated time points during starvation, cell–cell adhesion was assayed. (B) EDTA sensitive cell–cell adhesion. The graph represents the mean and standard error of three independent experiments ($*p < 0.05$, $**p < 0.01$). (C) A Western blot of CsaA showing delayed as well as decreased expression and a Western blot showing reduced CadA expression in $dio3^-$. Actin was used as a loading control. These experiments were repeated thrice ($n=3$).

but this is the first time its role has been reported in a lower eukaryote. In this study, we found that Dio3 controls growth, development, and cell-differentiation in *D. discoideum*. Specifically, Dio3 regulates cAMP relay and cell–cell adhesion. In mice, Dio3 is known to regulate growth and development by modulating active thyroxine levels (Hernandez et al., 2006).

D. discoideum Dio3 sequence subjected to protein–protein BLAST search against non-redundant sequences showed a 37% identity with the human Dio3 (accession number NP_001353.4) with an e-value of 7e − 22. pBLAST analysis confirmed that Dio3 of *Dictyostelium* belongs to the thioredoxin reductase superfamily (Fig. S1A), like all previously reported thyroxine deiodinases (Callebaut et al., 2003). Amino acid sequence alignment with pBLAST and SMART tools demonstrate that *D. discoideum* Dio3 contains a T4 deiodinase domain (Fig. S1B). These observed similarities between *D. discoideum* and vertebrates Dio3 suggest that *D. discoideum* Dio3 can be a vertebrate orthologue.

D. discoideum Dio3 shares a high degree of sequence identity with putative type III deiodinases from other slime molds: 63%, 59% and 58% with those of *P. pallidum*, *D. fasciculatum* and *D. purpureum*, respectively (Table S7). Selenocysteine encoded by the stop codon TGA is a typical signature of deiodinases and surprisingly, selenocysteine is absent in the other three slime molds mentioned above. The genomic DNA sequence of *D. discoideum dio3* has a TGA stop codon. To ascertain if TGA codes for a selenocysteine and forms a full length protein of Dio3, we made use of a highly conserved 3′ UTR regulatory region (the selenocysteine insertion sequence or SECIS; Lobanov et al., 2007; Zhang and Gladyshev, 2010). SECIS is responsible for recognizing TGA as selenocysteine. Based on the band size difference between Dio3:: GFP fusion protein and GFP fragments, we were able to ascertain that a full length Dio3 is indeed synthesized in *D. discoideum* (Fig. 2).

The $dio3^-$ cells were ineffective in moving towards folate (Videos S3, S4 and Fig. 7). This defective chemotaxis could explain the formation of small sized $dio3^-$ plaques. The speed at which cells join the aggregate can also influence aggregate size and development in *D. discoideum* (Jaiswal et al., 2012; Myers et al., 2005). Single cells as well as slugs of $dio3^-$ showed decreased motility during chemotaxis and phototaxis (Figs. 7 and 8) and this might be another reason for its delayed development.

In this study, reduced cAMP level at 8 h of development in $dio3^-$ suggests a weak cAMP relay in $dio3^-$ (Fig. 9A). As observed, $dio3^-$ has impaired aggregation and altered expression of *acaA*, *carA*, *pdsA*, *regA*, and *pde4* (Fig. 9B–F) thereby affecting other cAMP dependent processes. The strength of the cAMP relay is the initial factor that determines aggregation territory size (Gomer et al., 2011; Tang and Gomer, 2008). For example, $cnrN^-$ cells have excess cAMP levels that result in small territories and these can be rescued by starving cells at low density or by treating cells with a phosphodiesterase (Tang and Gomer, 2008). A weak cAMP relay and decreased cell movement are known to result in large aggregates and delayed development (Jaiswal et al., 2012). Disruption of any one of the genes involved in cAMP signaling such as *acaA*, *carA* and phosphodiesterases *pdsA*, *regA* and *pde4* genes results in aggregation defects in *D. discoideum* (Bader et al., 2006; Kim et al., 1998; Pitt et al., 1992; Sawai et al., 2007; Sucgang et al., 1997). Likewise, mutants that are defective in aggregate formation have defective expression of *acaA*, *carA*, *pdsA*, *regA*, and *pde4* (Garciandia and Suarez, 2013; Hirose et al., 2000; Rajawat et al., 2011; Wu and Janetopoulos, 2013).

Impaired cell–cell adhesion is known to manifest in aggregation defects (Kibler et al., 2003; Siu et al., 2004, 2011; Harloff et al., 1989; Loomis, 1988). The expression of CadA and CsaA is cAMP dependent (Siu et al., 2004; Yang et al., 1997). As the cAMP signal relay is affected in $dio3^-$, CadA and CsaA expression is also affected during early development. Altered CsaA and CadA expression has previously been shown to result in defective development (Garciandia and Suarez, 2013; Jaiswal et al., 2012; Mondal et al., 2007). Reduced cell–cell adhesion (Fig. 10A and B) might favor
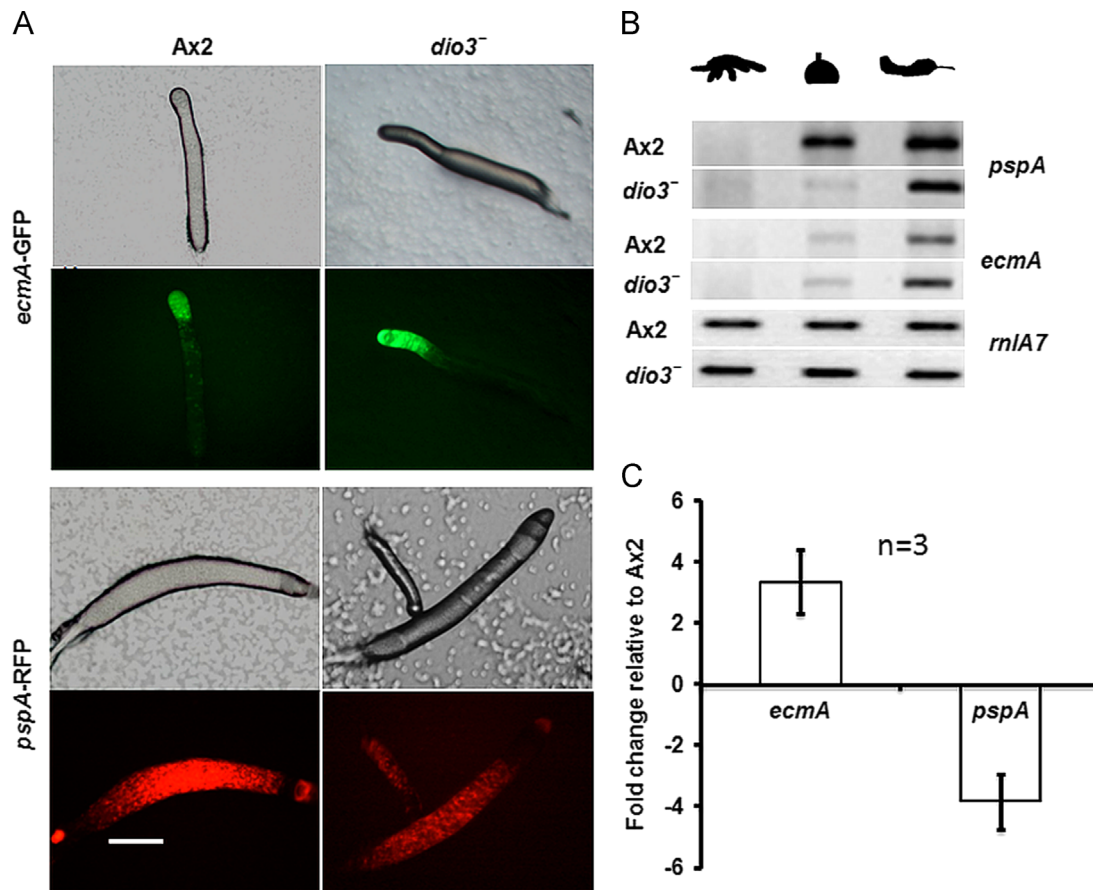
Fig. 11. Prestalk *ecmA* and prespore *pspA* expression patterns in Ax2 and *dio3⁻* slugs. (A) *ecmA* and *pspA* expression in Ax2 and *dio3⁻* slugs. Scale bar=200 μm. (B) Semi-quantitative PCR (RT-PCR) analyses of *ecmA* and *pspA* genes. RNA samples were prepared from aggregates, mounds and slugs of Ax2 and *dio3⁻* and used for RT-PCR in three independent experiments. In *dio3⁻*, *ecmA* expression was higher but *pspA* expression was reduced compared with Ax2. Equal amount of cDNA samples were used for all experiments and the PCR was carried out for 30 cycles. *rnlA* was used as control. Primer sequences are listed in Table S4. (C) ecmA and pspA expression in the slugs was quantified with ImageJ and the band intensities were normalized with *rnlA* expression levels. The mean and standard deviation is represented in the graph. The experiments were repeated thrice (*n*=3).

stream breaking, leading to small aggregate formation in *dio3⁻* (Kamboj et al., 1990; Roisin-Bouffay et al., 2000; Siu and Kamboj, 1990).

Cell-type differentiation in *D. discoideum* is also known to be regulated by extracellular cAMP levels (Anjard et al., 1997). Here we saw an impaired prestalk: prespore pattern in *dio3⁻* slugs and *ecmA* expression levels were higher compared with Ax2. Conversely, *pspA* expression was restricted to a smaller region in *dio3⁻* slugs (Fig. 11A). Further, differences in cell fate choices confirm that patterns in the *dio3⁻* slugs are abnormal. Presence of more *dio3⁻* cells in the prestalk region of chimeric slugs (Ax2:*dio3⁻*) implicate that Dio3 may be involved in promoting prespore identity (Fig. 12).

D. discoideum makes more than a dozen chlorinated compounds during development (Kay et al., 1992). A well characterized halogenated (chlorinated) compound is the differentiation-inducing factor 1 (DIF-1). Although it is produced by prespore cells, it promotes stalk cell differentiation (Kay and Thompson, 2001; Velazquez et al., 2011). Presumably, DIF-1 is degraded by the activity of dechlorinases (Velazquez et al., 2011). Several deiodinases have been shown to be involved in the dechlorination or debromination of halogenated compounds in other organisms (McTamney and Rokita, 2009). Therefore, with the induction of the prestalk cell-type in *dio3⁻*, we believe that *D. discoideum* Dio3 may be involved in the dechlorination of DIF-1 and act in parallel with DrcA (DIF-1 Reductive dechlorinase; DDB_G0293840). However, as observed by Velazquez et al. (2011), *dio3⁻* cells

surprisingly do not show any change in dechlorinase activity. Another possibility is that Dio3 may play a vital role in the dehalogenation of an unknown compound that is functionally identical to DIF-1. As seen in the amino acid sequence alignment of human and *D. discoideum* Dio3, the Dio3 active site is highly conserved. Hence, we believe that, *D. discoideum* Dio3 may also be involved in the deiodination of an unidentified "thyroxine like" or thyroxine molecule that is important for the cell growth and development.

Conclusions

This is the first report on characterization of Dio3 in a primitive eukaryote, *D. discoideum*. We found that *D. discoideum* and human Dio3 share homology in their active sites. Like human homolog, *D. discoideum* Dio3 has a selenocysteine residue in its active site. Surprisingly, Dio3 in other dictyostelids lacks selenocysteine. Our experiments demonstrate that *D. discoideum* synthesizes a full length Dio3 protein and it is expressed throughout development. At the slug stage Dio3 is enriched in the prespore region. Our experimental data support the role of *dio3* in the regulation of genes necessary for cAMP signaling, cell–cell adhesion, chemotaxis, and for cell-type patterning. The phenotype of *dio3⁻* strongly suggests that Dio3 may repress the formation of multiple signaling centers.
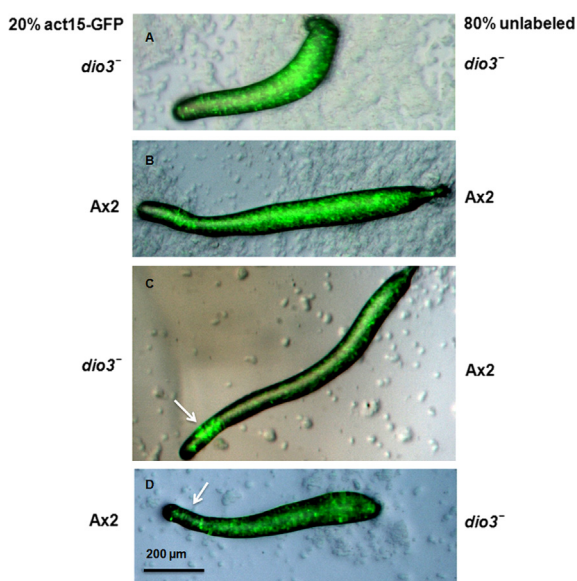
Fig. 12. Reconstitution of GFP-labeled Ax2 and *dio3⁻* cells. For chimeric slug formation and tracking the cell fate, Ax2 and *dio3⁻* cells were transfected with pTX-GFP vector. GFP marked and unmarked cells were mixed in a ratio of 20:80 and the GFP expression pattern was monitored in the slugs using a Nikon upright fluorescence microscope. (A) Chimeric slugs formed from GFP labeled Ax2 and unlabeled Ax2 cells showing uniform GFP distribution. (B) Slugs arising from reconstituted GFP labeled *dio3⁻* together with unlabeled *dio3⁻⁻* cells showing a uniform GFP pattern. (C) GFP labeled *dio3⁻* mixed with unlabeled Ax2 cells formed slugs with highly restricted GFP in the prestalk region (arrow). (D) GFP labeled Ax2 cells when mixed with unlabeled *dio3⁻* cells formed slugs with a higher fraction of GFP in the prespore part than unlabeled cells. Arrow indicates prestalk region. The experiments were repeated thrice ($n=3$). Scale bar $=200$ μm.

Author's contributions

SPS and RB designed the experiments. SPS performed all the experiments and analyzed data. RD helped SPS in the chemotaxis experiment and promoter reporter construction. SS performed the phototaxis assays light scattering. SPS wrote the manuscript, PJ, RD, ST, and RB edited the manuscript. All the authors read and approved the final manuscript.

Appendix A. Supporting information

Supplementary data associated with this article can be found in the online version at http://dx.doi.org/10.1016/j.ydbio.2014.10.012.

References

Anjard, C., van Bemmelen, M., Veron, M., Reymond, C.D., 1997. A new spore differentiation factor (SDF) secreted by Dictyostelium cells is phosphorylated by the cAMP dependent protein kinase. Differ.: Res. Biol. Divers. 62, 43–49.

Bader, S., Kortholt, A., Snippe, H., Van Haastert, P.J., 2006. DdPDE4, a novel cAMP-specific phosphodiesterase at the surface of dictyostelium cells. J. Biol. Chem. 281, 20018–20026.

Berry, M.J., Banu, L., Larsen, P.R., 1991. Type I iodothyronine deiodinase is a selenocysteine-containing enzyme. Nature 349, 438–440.

Bertholdt, G., Stadler, J., Bozzaro, S., Fichtner, B., Gerisch, G., 1985. Carbohydrate and other epitopes of the contact site A glycoprotein of Dictyostelium discoideum as characterized by monoclonal antibodies. Cell Differ. 16, 187–202.

Blagg, S.L., Stewart, M., Sambles, C., Insall, R.H., 2003. PIR121 regulates pseudopod dynamics and SCAR activity in Dictyostelium. Curr. Biol. 13, 1480–1487.

Bonner, J.T., 1967. The Cellular Slime Molds, Second ed. Princeton University Press, Princeton,, New Jersey.

Burrow, G.N., Fisher, D.A., Larsen, P.R., 1994. Maternal and fetal thyroid function. N. Engl. J. Med. 331, 1072–1078.

Callebaut, I., Curcio-Morelli, C., Mornon, J.P., Gereben, B., Buettner, C., Huang, S., Castro, B., Fonseca, T.L., Harney, J.W., Larsen, P.R., Bianco, A.C., 2003. The iodothyronine selenodeiodinases are thioredoxin-fold family proteins containing a glycoside hydrolase clan GH-A-like structure. J. Biol. Chem. 278, 36887–36896.

Desbarats, L., Brar, S.K., Siu, C.H., 1994. Involvement of cell-cell adhesion in the expression of the cell cohesion molecule gp80 in Dictyostelium discoideum. J. Cell Sci. 107 (Pt 6), 1705–1712.

Eichinger, L., Pachebat, J.A., Glockner, G., Rajandream, M.A., Sucgang, R., Berriman, M., Song, J., Olsen, R., Szafranski, K., Xu, Q., Tunggal, B., Kummerfeld, S., Madera, M., Konfortov, B.A., Rivero, F., Bankier, A.T., Lehmann, R., Hamlin, N., Davies, R., Gaudet, P., Fey, P., Pilcher, K., Chen, G., Saunders, D., Sodergren, E., Davis, P., Kerhornou, A., Nie, X., Hall, N., Anjard, C., Hemphill, L., Bason, N., Farbrother, P., Desany, B., Just, E., Morio, T., Rost, R., Churcher, C., Cooper, J., Haydock, S., van Driessche, N., Cronin, A., Goodhead, I., Muzny, D., Mourier, T., Pain, A., Lu, M., Harper, D., Lindsay, R., Hauser, H., James, K., Quiles, M., Madan Babu, M., Saito, T., Buchrieser, C., Wardroper, A., Felder, M., Thangavelu, M., Johnson, D., Knights, A., Loulseged, H., Mungall, K., Oliver, K., Price, C., Quail, M.A., Urushihara, H., Hernandez, J., Rabbinowitsch, E., Steffen, D., Sanders, M., Ma, J., Kohara, Y., Sharp, S., Simmonds, M., Spiegler, S., Tivey, A., Sugano, S., White, B., Walker, D., Woodward, J., Winckler, T., Tanaka, Y., Shaulsky, G., Schleicher, M., Weinstock, G., Rosenthal, A., Cox, E.C., Chisholm, R.L., Gibbs, R., Loomis, W.F., Platzer, M., Kay, R.R., Williams, J., Dear, P.H., Noegel, A.A., Barrell, B., Kuspa, A., 2005. The genome of the social amoeba Dictyostelium discoideum. Nature 435, 43–57.

Faix, J., Kreppel, L., Shaulsky, G., Schleicher, M., Kimmel, A.R., 2004. A rapid and efficient method to generate multiple gene disruptions in Dictyostelium discoideum using a single selectable marker and the Cre-loxP system. Nucleic Acids Res. 32, e143.

Fisher, P.R., 2001. Genetic Analysis of Phototaxis in Dictyostelium. Elsevier Science, Amsterdam.

Fisher, P.R., Annesley, S.J., 2006. Slug phototaxis, thermotaxis, and spontaneous turning behavior. Methods Mol. Biol. 346, 137–170.

Flegel, K.A., Pineda, J.M., Smith, T.S., Laszczyk, A.M., Price, J.M., Karasiewicz, K.M., Damer, C.K., 2011. Copine A is expressed in prestalk cells and regulates slug phototaxis and thermotaxis in developing Dictyostelium. Dev. Growth Differ. 53, 948–959.

Garcia, G.L., Rericha, E.C., Heger, C.D., Goldsmith, P.K., Parent, C.A., 2009. The group migration of Dictyostelium cells is regulated by extracellular chemoattractant degradation. Mol. Biol. Cell 20, 3295–3304.

Garciandia, A., Suarez, T., 2013. The NMRA/NMRAL1 homolog PadA modulates the expression of extracellular cAMP relay genes during aggregation in Dictyostelium discoideum. Dev. Biol. 381, 411–422.

Gaudet, P., Williams, J.G., Fey, P., Chisholm, R.L., 2008. An anatomy ontology to represent biological knowledge in Dictyostelium discoideum. BMC Genomics 9, 130.

Gomer, R.H., Jang, W., Brazill, D., 2011. Cell density sensing and size determination. Dev. Growth Differ. 53, 482–494.

Good, J.R., Kuspa, A., 2000. Evidence that a cell-type-specific efflux pump regulates cell differentiation in Dictyostelium. Dev. Biol. 220, 53–61.

Gregor, T., Fujimoto, K., Masaki, N., Sawai, S., 2010. The onset of collective behavior in social amoebae. Science 328, 1021–1025.

Guadano-Ferraz, A., Obregon St, M.J., Germain, D.L., Bernal, J., 1997. The type 2 iodothyronine deiodinase is expressed primarily in glial cells in the neonatal rat brain. Proc. Natl. Acad. Sci. USA 94, 10391–10396.

Harloff, C., Gerisch, G., Noegel, A.A., 1989. Selective elimination of the contact site A protein of Dictyostelium discoideum by gene disruption. Genes Dev. 3, 2011–2019.

Harris, E., Wang, N., Wu, Wl, W.L., Weatherford, A., De Lozanne, A., Cardelli, J., 2002. Dictyostelium LvsB mutants model the lysosomal defects associated with Chediak-Higashi syndrome. Mol. Biol. Cell 13, 656–669.

Hernandez, A., Martinez, M.E., Fiering, S., Galton St, V.A., Germain, D., 2006. Type 3 deiodinase is critical for the maturation and function of the thyroid axis. J. Clin. Investig. 116, 476–484.

Hirose, S., Inazu, Y., Chae, S., Maeda, Y., 2000. Suppression of the growth/differentiation transition in Dictyostelium development by transient expression of a novel gene, dia1. Development 127, 3263–3270.

Jaiswal, P., Soldati, T., Thewes, S., Baskar, R., 2012. Regulation of aggregate size and pattern by adenosine and caffeine in cellular slime molds. BMC Dev. Biol. 12, 5.

Jeanmougin, F., Thompson, J.D., Gouy, M., Higgins, D.G., Gibson, T.J., 1998. Multiple sequence alignment with Clustal X. Trends Biochem. Sci. 23, 403–405.

Kamboj, R.K., Lam, T.Y., Siu, C.H., 1990. Regulation of slug size by the cell adhesion molecule gp80 in Dictyostelium discoideum. Cell Regul. 1, 715–729.

Kay, R.R., Taylor, G.W., Jermyn, K.A., Traynor, D., 1992. Chlorine-containing compounds produced during Dictyostelium development. Detection by labelling with 36Cl. Biochem J. 281 (Pt 1), 155–161.

Kay, R.R., Thompson, C.R., 2001. Cross-induction of cell types in Dictyostelium: evidence that DIF-1 is made by prespore cells. Development 128, 4959–4966.

Kibler, K., Svetz, J., Nguyen, T.L., Shaw, C., Shaulsky, G., 2003. A cell-adhesion pathway regulates intercellular communication during Dictyostelium development. Dev. Biol. 264, 506–521.

Kim, J.Y., Borleis, J.A., Devreotes, P.N., 1998. Switching of chemoattractant receptors programs development and morphogenesis in Dictyostelium: receptor subtypes activate common responses at different agonist concentrations. Dev. Biol. 197, 117–128.

Knecht, D.A., Fuller, D.L., Loomis, W.F., 1987. Surface glycoprotein, gp24, involved in early adhesion of Dictyostelium discoideum. Dev. Biol. 121, 277–283.

Kohrle, J., 2000. The deiodinase family: selenoenzymes regulating thyroid hormone availability and action. Cell. Mol. Life Sci. 57, 1853–1863.

Kohrle, J., Rasmussen, U.B., Ekenbarger, D.M., Alex, S., Rokos, H., Hesch, R.D., Leonard, J.L., 1990. Affinity labeling of rat liver and kidney type I 5′-deiodinase. Identification of the 27-kDa substrate binding subunit. J. Biol. Chem. 265, 6155–6163.

Konijn, T.M., Chang, Y.Y., Bonner, J.T., 1969. Synthesis of cyclic AMP in Dictyostelium discoideum and Polysphondylium pallidum. Nature 224, 1211–1212.

Laevsky, G., Knecht, D.A., 2001. Under-agarose folate chemotaxis of Dictyostelium discoideum amoebae in permissive and mechanically inhibited conditions (1140–1142, 1144). BioTechniques 31, 1146–1149.

Langenick, J., Araki, T., Yamada, Y., Williams, J.G., 2008. A Dictyostelium homolog of the metazoan Cbl proteins regulates STAT signalling. J. Cell Sci. 121, 3524–3530.

Lee, S.K., Yu, S.L., Alexander, H., Alexander, S., 1998. A mutation in repB, the dictyostelium homolog of the human xeroderma pigmentosum B gene, has increased sensitivity to UV-light but normal morphogenesis. Biochim. Biophys. Acta 1399, 161–172.

Levi, S., Polyakov, M., Egelhoff, T.T., 2000. Green fluorescent protein and epitope tag fusion vectors for Dictyostelium discoideum. Plasmid 44, 231–238.

Lobanov, A.V., Fomenko, D.E., Zhang, Y., Sengupta, A., Hatfield, D.L., Gladyshev, V.N., 2007. Evolutionary dynamics of eukaryotic selenoproteomes: large selenoproteomes may associate with aquatic life and small with terrestrial life. Genome Biol. 8, R198.

Loomis, W.F., 1988. Cell-cell adhesion in Dictyostelium discoideum. Dev. Genet. 9, 549–559.

Luna, M., Guzman, G., Navarro, L., de la Pena, S.S., Valverde, R.C., 1995. Circadian rhythm of type II 5′deiodinase activity in the rat hypothalamic-pituitary-adrenal axis. Endocrine 3, 597–601.

Lusche, D.F., Rotzer, H., Merz, R., Fink, H., Mutzel, R., Schlatterer, C., 2004. Multichannel apparatus for parallel monitoring of light scattering in Dictyostelium discoideum cell suspensions. BioTechniques 37, 970–975.

McTamney, P.M., Rokita, S.E., 2009. A mammalian reductive deiodinase has broad power to dehalogenate chlorinated and brominated substrates. J. Am. Chem. Soc. 131, 14212–14213.

Mitra, R.S., Zhang, Z., Henson, B.S., Kurnit, D.M., Carey, T.E., D'Silva, N.J., 2003. Rap1A and rap1B ras-family proteins are prominently expressed in the nucleus of squamous carcinomas: nuclear translocation of GTP-bound active form. Oncogene 22, 6243–6256.

Mondal, S., Neelamegan, D., Rivero, F., Noegel, A.A., 2007. GxcDD, a putative RacGEF, is involved in Dictyostelium development. BMC Cell Biol. 8, 23.

Myers, S.A., Han, J.W., Lee, Y., Firtel, R.A., Chung, C.Y., 2005. A Dictyostelium homolog of WASP is required for polarized F-actin assembly during chemotaxis. Mol. Biol. Cell 16, 2191–2206.

Myre, M.A., Lumsden, A.L., Thompson, M.N., Wasco, W., MacDonald, M.E., Gusella, J.F., 2011. Deficiency of huntingtin has pleiotropic effects in the social amoeba Dictyostelium discoideum. PLoS Genet. 7, e1002052.

Ochiai, H., Stadler, J., Westphal, M., Wagle, G., Merkl, R., Gerisch, G., 1982. Monoclonal antibodies against contact sites A of Dictyostelium discoideum: detection of modifications of the glycoprotein in tunicamycin-treated cells. EMBO J. 1, 1011–1016.

Orozco, A., Valverde, R.C., Olvera, A., Garcia, G.C., 2012. Iodothyronine deiodinases: a functional and evolutionary perspective. J. Endocrinol. 215, 207–219.

Parkinson, K., Bolourani, P., Traynor, D., Aldren, N.L., Kay, R.R., Weeks, G., Thompson, C.R., 2009. Regulation of Rap1 activity is required for differential adhesion, cell-type patterning and morphogenesis in Dictyostelium. J. Cell Sci. 122, 335–344.

Pitt, G.S., Milona, N., Borleis, J., Lin, K.C., Reed, R.R., Devreotes, P.N., 1992. Structurally distinct and stage-specific adenylyl cyclase genes play different roles in Dictyostelium development. Cell 69, 305–315.

Rajawat, J., Mir, H., Begum, R., 2011. Differential role of poly(ADP-ribose) polymerase in D. discoideum growth and development. BMC Dev. Biol. 11, 14.

Raper, K.B., 1984. The Dictyostelids. Princeton University Press, Princeton, New Jersey.

Roisin-Bouffay, C., Jang, W., Caprette, D.R., Gomer, R.H., 2000. A precise group size in Dictyostelium is generated by a cell-counting factor modulating cell-cell adhesion. Mol. Cell 6, 953–959.

Rost, B., Yachdav, G., Liu, J., 2004. The PredictProtein server. Nucleic Acids Res. 32, W321–326.

Salvatore, D., Low, S.C., Berry, M., Maia, A.L., Harney, J.W., Croteau St, W., Germain, D.L., Larsen, P.R., 1995. Type 3 Iodothyronine deiodinase: cloning, in vitro expression, and functional analysis of the placental selenoenzyme. J. Clin. Investig. 96, 2421–2430.

Saran, S., Meima, M.E., Alvarez-Curto, E., Weening, K.E., Rozen, D.E., Schaap, P., 2002. cAMP signaling in Dictyostelium. Complexity of cAMP synthesis, degradation and detection. J. Muscle Res. Cell Motil. 23, 793–802.

Sawai, S., Guan, X.J., Kuspa, A., Cox, E.C., 2007. High-throughput analysis of spatiotemporal dynamics in Dictyostelium. Genome Biol. 8, R144.

Schmittgen, T.D., Livak, K.J., 2008. Analyzing real-time PCR data by the comparative C(T) method. Nat. Protoc. 3, 1101–1108.

Schultz, J., Milpetz, F., Bork, P., Ponting, C.P., 1998. SMART, a simple modular architecture research tool: identification of signaling domains. Proc. Natl. Acad. Sci. USA 95, 5857–5864.

Shaulsky, G., Fuller, D., Loomis, W.F., 1998. A cAMP-phosphodiesterase controls PKA-dependent differentiation. Development 125, 691–699.

Simpson, P.A., Spudich, J.A., Parham, P., 1984. Monoclonal antibodies prepared against Dictyostelium actin: characterization and interactions with actin. J. Cell Biol. 99, 287–295.

Siu, C.H., Harris, T.J., Wang, J., Wong, E., 2004. Regulation of cell-cell adhesion during Dictyostelium development. Semin. Cell Dev. Biol. 15, 633–641.

Siu, C.H., Kamboj, R.K., 1990. Cell-cell adhesion and morphogenesis in Dictyostelium discoideum. Dev. Genet. 11, 377–387.

Siu, C.H., Sriskanthadevan, S., Wang, J., Hou, L., Chen, G., Xu, X., Thomson, A., Yang, C., 2011. Regulation of spatiotemporal expression of cell-cell adhesion molecules during development of Dictyostelium discoideum. Dev. Growth Differ. 53, 518–527.

Sucgang, R., Weijer, C.J., Siegert, F., Franke, J., Kessin, R.H., 1997. Null mutations of the Dictyostelium cyclic nucleotide phosphodiesterase gene block chemotactic cell movement in developing aggregates. Dev. Biol. 192, 181–192.

Tang, Y., Gomer, R.H., 2008. A protein with similarity to PTEN regulates aggregation territory size by decreasing cyclic AMP pulse size during Dictyostelium discoideum development. Eukaryot. Cell 7, 1758–1770.

Velazquez, F., Peak-Chew, S.Y., Fernandez, I.S., Neumann, C.S., Kay, R.R., 2011. Identification of a eukaryotic reductive dechlorinase and characterization of its mechanism of action on its natural substrate. Chem. Biol. 18, 1252–1260.

Waterhouse, A.M., Procter, J.B., Martin, D.M., Clamp, M., Barton, G.J., 2009. Jalview Version 2—a multiple sequence alignment editor and analysis workbench. Bioinformatics 25, 1189–1191.

Wessels, D., Srikantha, T., Yi, S., Kuhl, S., Aravind, L., Soll, D.R., 2006. The Shwachman-Bodian-Diamond syndrome gene encodes an RNA-binding protein that localizes to the pseudopod of Dictyostelium amoebae during chemotaxis. J. Cell Sci. 119, 370–379.

Williams, J.G., 2006. Transcriptional regulation of Dictyostelium pattern formation. EMBO Rep. 7, 694–698.

Wu, Y., Janetopoulos, C., 2013. Systematic analysis of gamma-aminobutyric acid (GABA) metabolism and function in the social amoeba Dictyostelium discoideum. J. Biol. Chem. 288, 15280–15290.

Yang, C., Brar, S.K., Desbarats, L., Siu, C.H., 1997. Synthesis of the Ca(2+)-dependent cell adhesion molecule DdCAD-1 is regulated by multiple factors during Dictyostelium development. Differ.: Res. Biol. Divers. 61, 275–284.

Zhang, Y., Gladyshev, V.N., 2010. General trends in trace element utilization revealed by comparative genomic analyses of Co, Cu, Mo, Ni, and Se. J. Biol. Chem. 285, 3393–3405.